Available online at www.sciencedirect.com
SCIENCE DIRECT®
Polymer 44 (2003) 5355–5367
polymer
www.elsevier.com/locate/polymer

The role of crystallinity in the crystallographic texture evolution of polyethylenes during tensile deformation

D.S. Li[a,1], H. Garmestani[a,*,1], R.G. Alamo[b,*], S.R. Kalidindi[c]

[a]*Department of Mechanical Engineering, Center for Materials Research and Technology, Florida Agricultural and Mechanical University and Florida State University College of Engineering, Florida State University, Tallahassee, FL 32310-6046, USA*
[b]*Department of Chemical Engineering, Florida Agricultural and Mechanical University and Florida State University College of Engineering, Tallahassee, FL 32310-6046, USA*
[c]*Department of Materials Engineering, Drexel University, Philadelphia, PA 19104, USA*

Received 27 January 2003; received in revised form 4 June 2003; accepted 6 June 2003

Abstract

The crystallographic texture evolution of rapidly crystallized high-density polyethylene (HDPE) and ethylene-1-octene copolymer prepared with a Ziegler–Natta (LLDPE) catalyst, was studied during tensile deformation using wide-angle X-ray diffraction WAXD. The popLA software suite, a methodology based on spherical harmonics for texture analysis, was utilized to produce recalculated pole figures and orientation distribution function plots from the raw data. An important aspect of this work has been the in situ measurement of texture during tensile deformation and the subsequent measurement of texture in the relaxed samples. The difference in molecular structure of the polyethylenes had a strong effect in the initial texture as well as in the rate of texture evolution during deformation. Texture evolves slowly in the HDPE while a fast drastic change in texture is observed in LLDPE after yield. At higher strains the texture of LLDPE was basically unchanged revealing not only a strong (100)[001] '*c*-axis' texture component, but also other weaker texture components such as (010)[001], (1×0)[010], (011)[100] and (201)[$\bar{1}$02]. Furthermore, while relaxation after unloading mitigated or eliminated two of the preferred texture components in HDPE strengthening the (001) component aligned along the extension axis, it was observed that the texture of LLDPE did not undergo any significant changes after relaxation. At large strains ($\varepsilon > 1.0$), microfibers formed in both HDPE and LLDPE. A lamellar substructure that differs between the HDPE and LLDPE is observed by AFM images of drawn materials. The role of possible slip mechanisms and stress relaxation in the evolving crystallographic texture of these polyethylenes is discussed.

Keywords: Polyethylenes; Tensile deformation; Morphology

1. Introduction

Polyethylene products, in a variety of forms ranging from fibers to sheets are manufactured through a series of thermo-mechanical treatments. Different processes results in different microstructures, and consequently differing properties in the final products. There has therefore been an increasing interest in understanding the details of the evolution of microstructure during processing among the mechanics and materials community [1–9].

Tensile deformation of a semicrystalline polymeric material occurs through three major steps. An initial reversible elastic response is followed by a region of large deformation with only a small increase in stress and by a third region before break (strain hardening) where deformation is limited and a fiber like structure is fully developed [3,4,10–12]. Deformation occurs mainly in the amorphous regions during the elastic regime and crystalline and amorphous regions cooperatively deform primarily via intra and inter-crystalline slips from the early stages of the second regime of deformation, i.e. just after yield. Chain slip is generally the easiest system to be activated and crystallographic and interlamellar slips lead to segmentation of the original (lamellar) crystallites. Hence, smaller blocks

* Corresponding authors. Address: Florida Agricultural and Mechanical University and Florida State University College of Engineering, Tallahassee, FL 32310-6046, USA.
E-mail addresses: hamid.garmestani@mse.gatech.edu (H. Garmestani), alamo@eng.fsu.edu (R.G. Alamo).
[1] Present address: Department of Materials Engineering, Georgia Institute of Technology, Atlanta, GA 30332.

0032-3861/03/$ - see front matter © 2003 Published by Elsevier Ltd.
doi:10.1016/S0032-3861(03)00527-5

of crystallites translate and reorient preferentially in the direction of elongation to end in a fiber-like, highly textured structure during the last stages of the second regime of deformation. Further deformation of the highly oriented structure is energetically costly and eventually leads to bond breakage and failure.

Although these general deformation paths could be ascribed to semicrystalline polyethylenes, the details of the deformation process are, however, a function of the polyethylene chain microstructure and the initial crystallite morphology. It is expected that the transitory stages that allow crystallites with a favorable orientation for slip would depend on the initial phase structure, contributing to the complexities in establishing mechanisms of deformation in these systems. An important microstructural detail of the crystalline region is the distribution of crystal lattice orientations in the specimen of interest (also referred to as crystallographic texture or simply texture). Wide angle X-ray pole figure analysis provides stereographic projection of diffraction planes as a function of their orientation within the sample.

Texture development in low density polyethylene (LDPE) during tensile deformation was studied by Pazur et al. [5]. The authors obtained data in the form of pole figures in a strain relaxed mode (allowing one month of relaxation after uniaxial extension). Three distinct regions were found in the stress–strain curve. Prior to deformation, the samples exhibited a weak *b*-axis orientation along the normal direction. At the onset of yielding, in addition to the *c*-axis orientation along the extension direction, an *a*-axis texture component developed and quickly diminished. As the samples were stretched further, a dominant **c**-axis fiber component developed. Pole figures or texture data that would correspond to the actual deformed state, prior to relaxation, were not provided. Akin to the work by Pazur et al. [5], most prior studies on the details of texture evolution of polyethylenes were carried out ex situ and did not isolate the relaxation process from deformation [1,2,5]. Only a few in situ studies of high density and linear low-density polyethylenes were conducted using simultaneous SAXS/WAXD measurements [3,4,6,7–9]. However, the latter works did not include measurements of the evolution of texture.

In a previous study [13], we reported in situ texture evolution of high-density polyethylene (HDPE) during tensile deformation. Using methods based on spherical harmonics, the pole figures at different strains were recalculated. Interestingly, in agreement with other TEM studies [14], the pole figures of HDPE deformed to large strains suggested that the deformed polyethylene retained traces of the initial texture. The preferred deformation texture components in HDPE appeared to be (001), near-(011), and (010) fiber components. The (001) fiber is the strongest deformation texture component in HDPE, and the other two components continued to be present even at the highest strains. However, when the samples were allowed to relax, a strong *c*-axis fiber component dominated the texture results and the other components weakened considerably.

The present study was prompted by the lack of texture analysis in linear low density polyethylenes (LLDPE) subject to uniaxial tension and our observation that relaxation played an important role in the texture evolution of polyethylenes. Pole figure analysis of texture evolution was carried out for a Ziegler–Natta type ethylene-1-octene copolymer. The branched nature of this copolymer restricts crystallinity and gives a completely different initial texture (closer to a random texture) to that of the HDPE previously studied [13]. Therefore, the effect of molecular structure (or crystallinity) on the texture evolution can be comparatively evaluated. The texture was analyzed during deformation under load and after relaxation and the lamellar structure of deformed and relaxed specimens was subsequently imaged by atomic force microscopy (AFM). Attempts are made to describe the evolution of the lamellar morphology during uniaxial deformation in both types of polyethylenes. The differences in textural and relaxation behavior of HDPE and LLDPE during deformation are correlated with the microstructures of these two materials and their mechanical behavior. It will be shown that the relaxation behavior of the LLDPE (and its differences to HDPE) determines the nature of the texture evolution and it can be concluded that deformation mechanisms responsible for texture changes may not be different for these polyethylenes.

2. Experimental methods

The polyethylenes used in this study were a commercial high density polyethylene (HDPE) made by the Phillips process and a heterogeneous linear low density polyethylene (LLDPE) synthesized with a Ziegler–Natta type catalyst by the DOW Chemical Co. The molecular characterization and thermal data of the as-prepared and fully deformed polyethylenes are listed in Table 1. Melting behaviors were measured in a Perkin–Elmer DSC-7 calorimeter at 10 °C/min and degrees of crystallinities obtained from the measured heat of fusion (ΔH), using 290 J/g as the heat of fusion of pure orthorhombic polyethylene crystallites.

Dumbbell shaped tensile specimens were obtained by compression molding using a methodology described in our prior work [13]. Films were prepared in a Carver press at about 175 °C and a pressure of 150 atm. The molten film was held for about 10 min and then rapidly quenched in water at 23 °C. The specimens used are schematically shown in Fig. 1 and had the following dimensions: length of 140 mm, thickness of 0.45 mm and gauge dimensions of 80 mm (L) × 15 mm (W). Sample coordinate axes are also labeled in Fig. 1, ED as extension direction, TD as transverse direction that lies on the surface of the sample while normal to the extension direction and ND as the normal direction, perpendicular to the specimen surface.

Table 1
Molecular characterization of polyethylenes studied

Sample	M_w	M_w/M_n	Branching (mol%)	T_m (°C)	ΔH (J/g)	$X_{(\Delta H)}$
HDPE	127,000	13.3	–	130.0[a] 134.1[b]	200[a] 210[b]	0.69
LLDPE (1-octene based)	88,700	5.4	2.03	120.0[a] 121.0[b]	131[a] 143[b]	0.45

[a] Undeformed.
[b] Deformed ($\varepsilon \sim 7.0$) and relaxed.

Mechanical tests were carried out using a screw driven Model 1011 Instron tensile machine. All samples were deformed at ambient temperature (24–26 °C) at a strain rate of 0.0033 (inch/inch) sec^{-1} (corresponding to an extension rate of 5 mm/min). The actuator was stopped after reaching a desired strain level and, while under load, a special fixture was attached to the sample to maintain it at a constant extension level. A schematic diagram of this fixture was given in a previous work [13]. The sample with the attached fixture was then taken out of the Instron machine and placed directly in the X-ray goniometer to perform texture analysis. The device ensures that deformed polyethylene exposed to the X-ray beam will maintain a constant total strain during texture measurements. Although the device does not prevent the occurrence of local straining, the inelastic strain is ensured not to exceed the elastic strain of the sample during the measurement.

Texture in the initial and the deformed samples were measured by wide angle X-ray diffraction (WAXD). After the texture measurement was completed, the samples were taken out of the special fixture and allowed to relax for 3 days. Then the texture of the relaxed samples was studied again. The X-ray facility used is a Philips X'Pert PW3040 MRD X-ray diffractometer, equipped with a pole figure goniometer, operating at 40 kV and 45 mA and employing Ni filtered Cu Kα radiation. Incomplete pole figures were obtained from the projections of sample orientation with respect to the incident beam, with α angle varying from 0 to 85° in 5° intervals and β angle varying from 0 to 360° in 5° steps. The following reflections were analyzed to determine texture components: (110), (200), (020), (011), (201). The diffraction data was corrected for geometric defocusing and background X-ray intensity using standard procedures. The

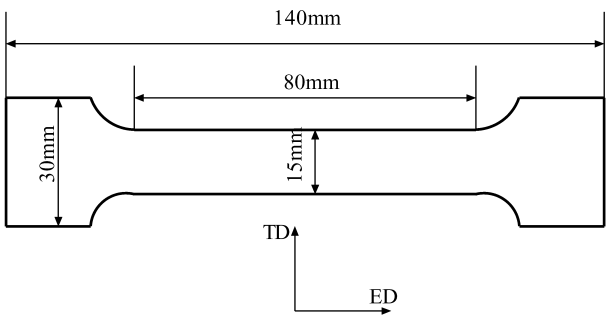

Fig. 1. Schematic illustration of the tensile specimen used.

crystallographic unit cell of polyethylene is orthorhombic with known lattice constants of $a = 0.741$ nm; $b = 0.495$ nm; and $c = 0.255$ nm [15]. The polymer chain lies parallel to the c-axis.

A harmonic algorithm implemented in the preferred orientation software package from Los Alamos (popLA) [16] was initially used to calculate the coefficients of the crystallite orientation distribution function. In a second step the coefficients are used as input in the popLA software to recalculate any pole figure and the crystallite orientation function (ODF). The procedure to reconstruct the experimental pole figures from the specimen orientation distribution was explained in the earlier work [13]. A great advantage of this method is the possibility of reconstructing any pole figure. For example, the important (002) c-axis pole figure, which is difficult to be measured by direct analysis, can be easily generated by this method.

ODF plots are also presented in this study as plots of the probabilities in Eulerian space for different constant φ sections. The texture components for orthorhombic materials can be considered in terms of ideal orientations (hkl)[uvw] using the Miller index nomenclature. An ideal orientation can be found from known Euler angles (θ, φ, ψ) using the relations:

$$h = -a\sin\theta\cos\varphi \tag{1-a}$$

$$k = b\sin\theta\sin\varphi \tag{1-b}$$

$$l = c\cos\theta \tag{1-c}$$

$$u = \frac{1}{a}(\cos\psi\cos\theta\cos\varphi - \sin\psi\sin\varphi) \tag{1-d}$$

$$v = \frac{1}{b}(-\cos\psi\cos\theta\sin\varphi - \sin\psi\cos\varphi) \tag{1-e}$$

$$w = \frac{1}{c}\cos\psi\sin\theta \tag{1-f}$$

In an effort to understand the relaxation rate constants, measurement of the stress relaxation was conducted on both polyethylenes. In these tests, the samples were deformed up to a strain of 1.0 at a strain rate of 0.0033 sec^{-1} and held at that strain while the decay of the stress was monitored during 4 h.

The lamellar morphology of the surface of undeformed and deformed specimens was imaged by AFM using a JEOL 4210 instrument. An Olympus brand silicon tip oscillating slightly below its resonance frequency (~300 kHz) was

used to scan the sample by a non-contact mode. The output images were collected in the form of topography images and phase images simultaneously. In selected samples the aluminum foil used to line the plates holding the mold was replaced by mica to minimize surface roughness. The details of the crystalline morphology were, in the specimens prepared within aluminum foil, enhanced by etching the films in a 1% w/v solution of potassium permanganate dissolved in a previously prepared acid–water mixture. This mixture was made from 10 parts sulfuric acid, 4 parts *ortho*-phosphoric acid and 1 part water according to the procedure of Olley et al. [17]. Etching time was 30 min for both polyethylenes. The etching mixture was thoroughly rinsed with a solution of 1 part hydrogen peroxide in a 2:7 mixture of sulfuric acid and water. The film was washed in distilled water and then dried in vacuum before imaging. The specimens prepared on mica surfaces were directly observed by AFM without any etching treatment.

3. Results and discussion

3.1. Texture evolution during deformation

Engineering stress (σ)–strain (ε) curves up to fracture are shown in Fig. 2(a) for both polyethylenes. The large differences observed in the yield patterns of both polyethylenes have been correlated with the different crystallinity levels [18–20]. HDPE with a crystallinity of 69% displays a sharp single high yield stress compared to the much lower and broader yield of the copolymer with only 45% crystallinity. Failure takes place at deformations of 700–800% for both materials. From these data the corresponding true stress ($\sigma_T = \sigma(1+\varepsilon)$)–true strain ($\varepsilon_T = \ln(1+\varepsilon)$) curves were calculated and are shown in Fig. 2(b). In the latter types of plots the differences in yield stress observed in Fig. 2(a) are diminished and the regime of plastic flow from the yield point to fracture is very similar in both polyethylenes. This similarity in true stress-true strain behavior was also observed by Hiss et al. [8] in a more extended series of different types of polyethylenes. These authors implemented on-line corrections to acquire load - displacement data at a true constant strain rate. In spite of differences in crystallinities, it was concluded that the deformation process of the various polyethylenes had the same general behavior. The true stress-true strain curves of HDPE and an ethylene copolymer with similar branching content to the LLDPE studied in this work are remarkably similar to the curves of Fig. 2(b). It is important to note that the experimental data reported here and plotted in Fig. 2(b), were obtained at constant extension rate (not constant true strain rate).

The evolution of texture of the same linear polyethylene (HDPE) at different strains was reported in our previous paper [13]. Thus, we focus in this work in the in situ experimental observation of the texture measurements on

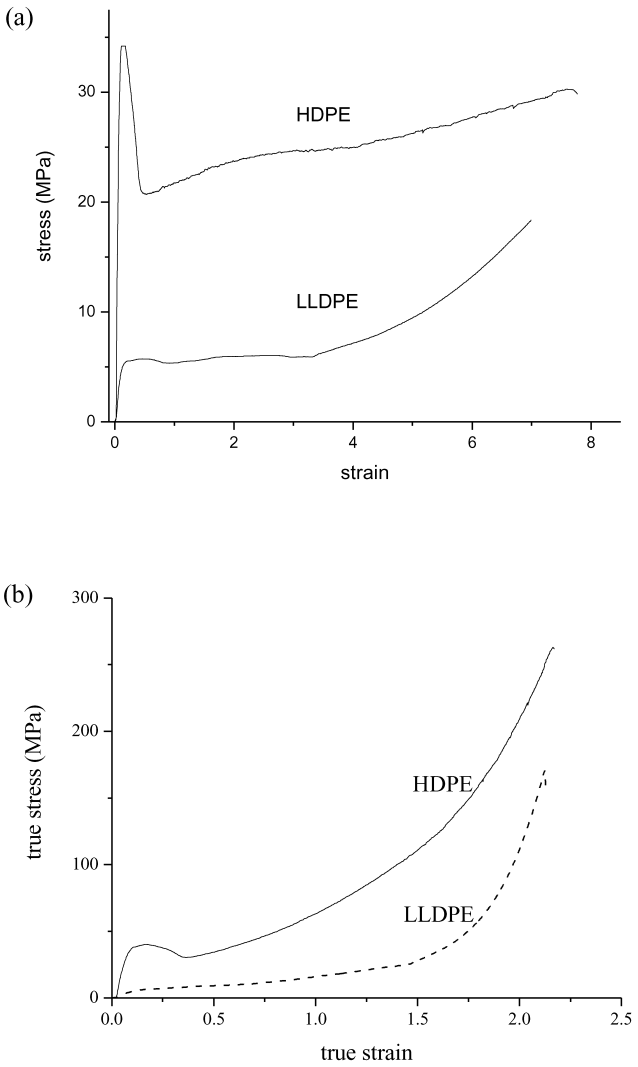

Fig. 2. (a) Engineering stress–strain relaxation of HDPE and LLDPE. (b) True stress vs. true strain of the same polymers.

the ethylene 1-octene copolymer under deformation. Data of the linear polymer will be also presented for a comparative analysis of the texture during deformation of both types of polyethylenes. The recalculated (100), (010) and (001) pole figures for un-deformed ethylene l-octene copolymer and deformed to strains (ε) of 1.0, 4.0 and 6.0 are given in Fig. 3(a)–(d) respectively. All pole figures are plotted in a stereographic projection with a log intensity scale. A density of one in the scale corresponds to a random distribution. Calculated pole densities are plotted in units of times random distribution. The initial un-deformed LLDPE has a very light texture as seen in Fig. 3(a), with a weak preferred orientation of the crystallographic planes of approximately 1.5 times random. From the (100) pole figure, we noticed the *a*-axis weakly distributed along the ED/TD plane. Diffraction from the (010) plane shows a weak *b*-axis orientation along the normal direction. Correspondingly, the (001) pole shows that the *c*-axis is distributed in the ED/TD plane. The initial LLDPE texture is similar to that of the

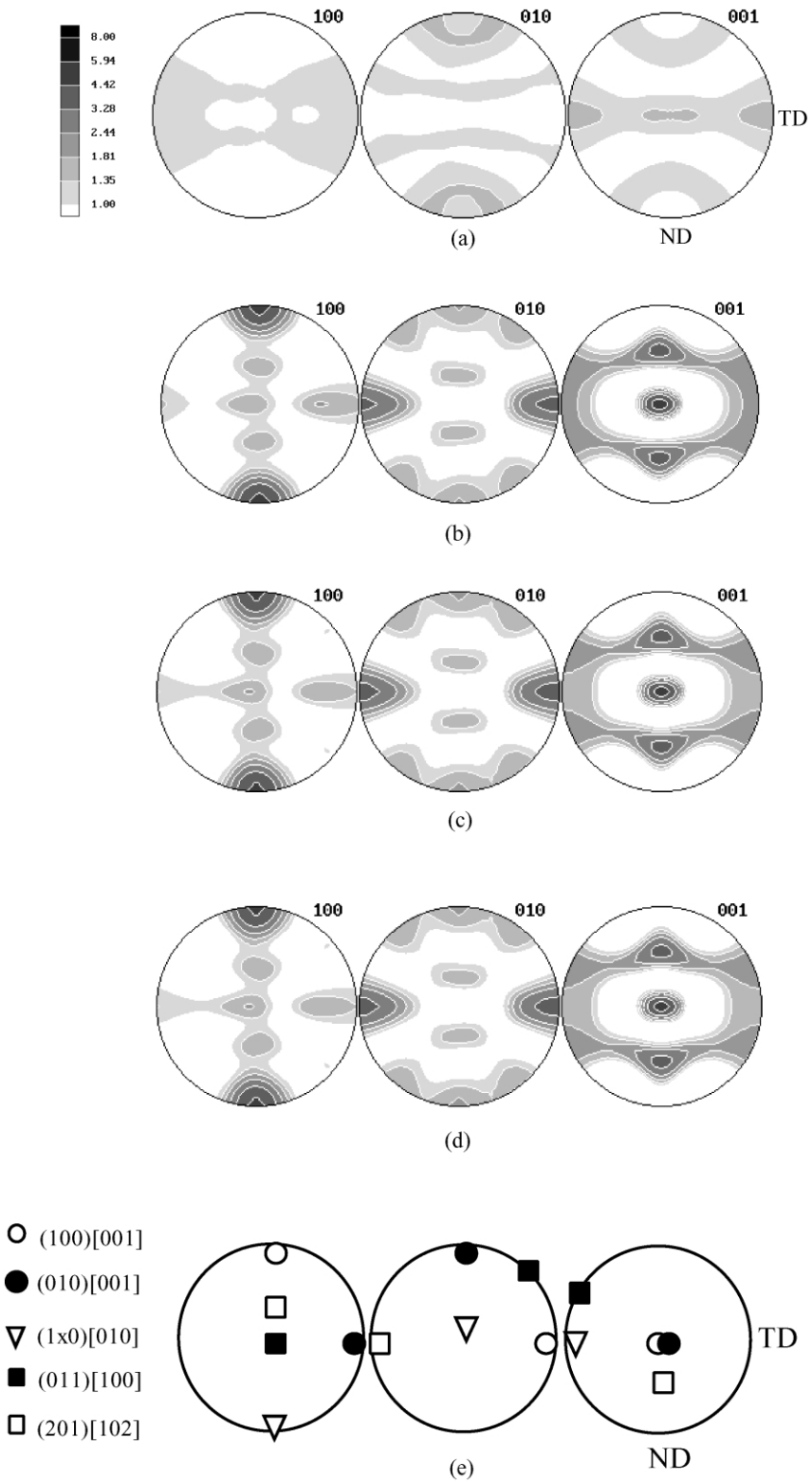

Fig. 3. Pole figures of the (100), (010), (001) planes of orthorhombic crystals of un-deformed and deformed ethylene 1-octene copolymer at different strains (ε). (a) $\varepsilon = 0$. (b) $\varepsilon = 1.0$, (c) $\varepsilon = 4.0$, (d) $\varepsilon = 6.0$, (e) projection of texture components for $\varepsilon = 1$.

un-deformed LDPE studied by Pazur et al. [5], but clearly different from that of HDPE [13]. The morphology of this weakly textured LLDPE is shown in Fig. 4. A 20×20 μ AFM image of an etched film (Fig. 4(a)) reveals banded spherulites of ~5 μm diameter and about 0.5 μm band spacing. Fig. 4(b) shows a 2×2 μ image of the center of one of the spherulites. Edge and flat-on lamellae with apparent nodular structure are observed to be radially

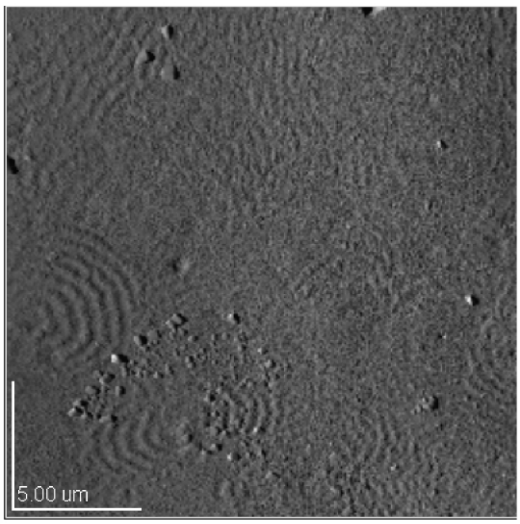

(a)

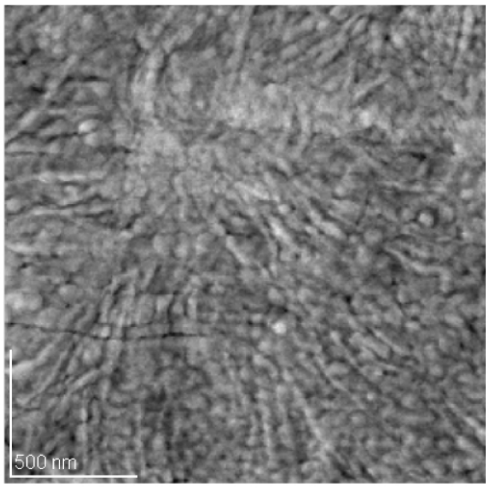

(b)

Fig. 4. AFM images of un-deformed LLDPE. (a) 20 μ image of etched film with clear banded spherulites present. (b) Lamellar structure of central region of the spherulites. Image was taken in un-etched film.

distributed. The texture and spherulitic morphology of LLDPE stretched to a strain of 0.08, within the elastic region, were basically identical to Figs. 3(a) and 4(a). Only a minor deformation of the spherulites in the direction of elongation was noticed in the AFM micrographs. It is observed that up to the yield point the initial LLDPE crystalline structure and texture is mainly preserved in agreement with the reversibility of the deformation process in this region.

Fig. 3(b)–(d) document the texture evolution of the ethylene l-octene copolymer past the yield point and up to large strains in uniaxial tension. The similarity of the pole figures in the whole range of plastic deformation is remarkable. From the initial stages of the plastic region there are no remnants of the weak texture initially present in the un-deformed sample. Five new texture components prevail and their intensity remains constant with small changes during the whole plastic deformation. This behavior is quite different from the uniaxial deformation of highly crystalline HDPEs in which the texture was observed to evolve slowly during the plastic regime and even after a strain of 7.2, the initial texture components were still present to a significant degree [13].

The individual texture components identified by texture analysis are schematically shown in Fig. 3(e). These same components are also shown in the Orientation Distribution (OD) plots in Fig. 5. The OD plots were constructed by mapping 2D sections of orientation distribution calculated at different Euler angles as shown in Fig. 5 for $\varphi = 0°$ and $\varphi = 90°$. The components are assigned to the pole regions of the pole figure plots as shown in Fig. 3(e). The Euler angles of the five components of the texture are listed in Table 2.

Among these five new components, shown in Fig. 3, texture component (100)[001] is the most prominent and the strongest. Its *c*-axis is aligned with the sample extension, the *b*-axis with the transverse direction and the *a*-axis with the normal direction. From the texture analysis (as shown in Fig. 5) we find the intensity for this component to be 8 times random. This component has been attributed to chain slip [28]. An additional weaker (010)[001] component is also present with an intensity of about 5.0 times random. In this component the *b*-axis is aligned with the normal direction while the *c*-axis is aligned with the extension direction. Texture analysis reveals the existence of a component defined here as $(1 \times 0)[010]$, which is recognized as a rotation of 5° from the transverse direction (100)[010]. Two other components are also identified as (011)[100] and (201)[$\bar{1}$02].

X-ray pole figures of the uniaxial tension deformation of ethylene copolymers were previously studied only in samples crystallized from oriented melts, such as blown films of LDPE [5] or LLDPE [21,22]. Pazur et al. [5] carried out simple pole figure analysis and for high draw ratios the observed texture was consistent with a single main uniaxial (100) fiber component, which was associated with the presence of a fibrillar morphology. Additional texture components were not observed. Hence, either the initially oriented morphology contributed to the formation of a more textured fibrillar structure at high strains or perhaps weaker components, misaligned with the elongation direction, are only observed when *rigorous* methods of texture analysis are used to recalculate the most significant pole figures. Moreover, the texture was not measured while the sample was kept in the deformed state. The work of Butler et al. [22] in blown and cast LLDPE films followed a pole figure treatment similar to that used in our study, i.e. orientation distributions were analyzed from the recalculated (002) pole figures. These authors identified differences in orientation distributions between both film processes, which were correlated with differences in properties of both films.

Also of relevance is the study of the 'in situ' deformation of LLDPEs by Donalds et al. [3,9] who measured simultaneous small- and-wide angle X-ray scattering during

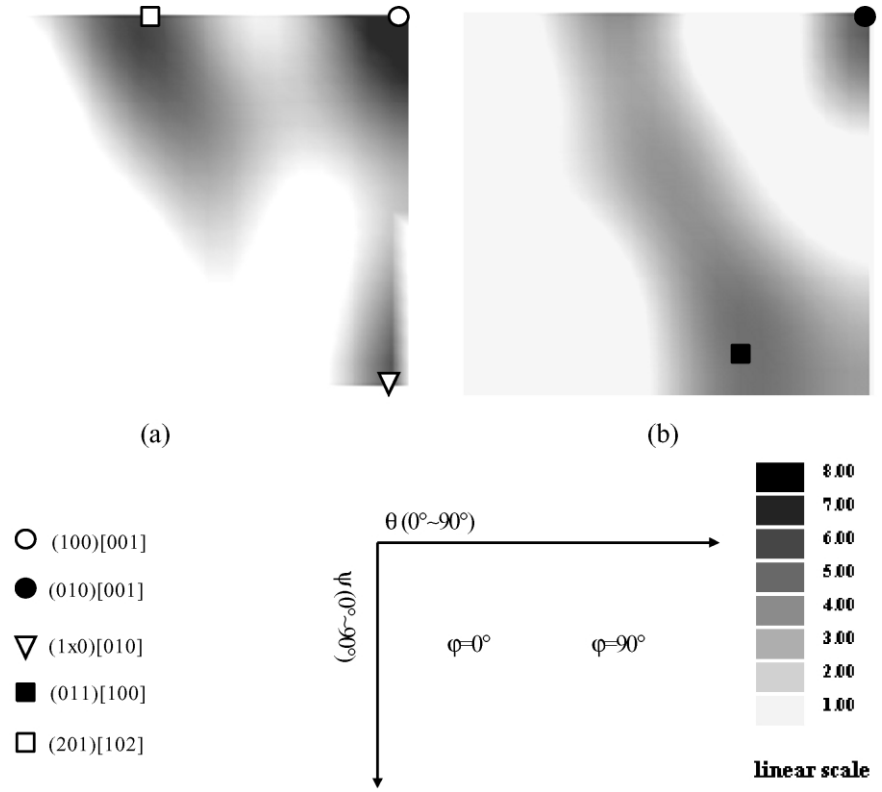

Fig. 5. ODF plot for ethylene-1-octene copolymer at a strain of 1.0 on fixture. (a) 2D projection at $\varphi = 0°$. (b) 2D projection at $\varphi = 90°$.

uniaxial tensile deformation. Time resolved experiments were instrumental to identify a reversible martensitic transformation at the yield point by the appearance of the monoclinic (001) reflection. This reflection disappeared when the samples were allowed to relax and was associated with reversible fine chain slip in the elastic deformation. It is not unusual that we do not observe traces of the monoclinic reflection because, as we will show later, most of the stress in the deformed LLDPE studied here relaxes prior to our WAXD data acquisition (although the total strain on the sample was kept constant). The constancy of texture and morphology of LLDPE during deformation in the elastic region is in agreement with the results of Donalds et al. for similar types of polyethylenes. The disappearance of the meridional long spacing at the end of the yield region was associated with the irreversible lamellar fragmentation that precedes coarse intra-lamellar chain slip and the beginning of the fibrillar texture according to Peterlin's model of deformation [10]. The drastic change in the pole figures of Fig. 3 before and after yield of LLDPE and the presence of a strong (100)[001] component are also consistent with considerable interlamellar slip and orientation through the chain *c*-axis.

The evolution of the lamellar morphology during deformation was followed by AFM imaging of the film surface. Images of the ethylene 1-octene copolymer stretched to a strain of 1.0 and 6.0 and partially held under load using a Kraton film are given in Fig. 6(a),(b), respectively. The AFM images show elongated and twisted fibers of about 0.1 μ diameter, which are clearly formed from the initial stages of the plastic region. With increasing strain, longitudinally, the fibers develop a granular appearance possibly from the increasing role of inter-lamellar slippage at these stages of deformation (Fig. 6(b),(c)). The effect of strain relaxation on the fibrillar morphology of LLDPE are revealed in the AFM images of Fig. 7 (a),(b) for the fully relaxed copolymer which was previously deformed to a strain of 6.0. The changes are remarkable and the

Table 2
Euler angles in degrees corresponding to the different texture components observed in this study

Euler angle	Texture component				
	(100)[001]	(010)[001]	(1 × 0)[010]	(011)[100]	(201)[$\bar{1}$02]
Φ	0	90	0	90	0
θ	90	90	85	60	35
ψ	0	0	90	85	0

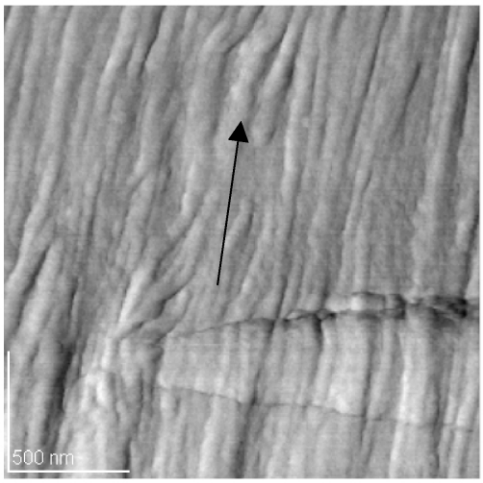

(a)

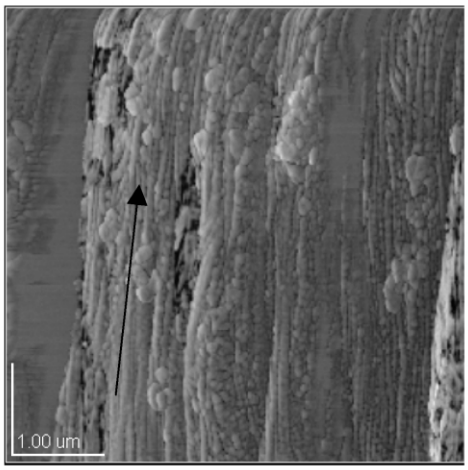

(b)

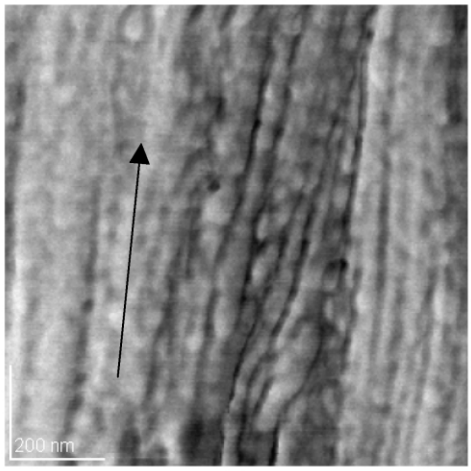

(c)

Fig. 6. AFM images of fibrillar structure of deformed LLDPE. (a) $\varepsilon = 1.0$, (b) $\varepsilon = 6.0$, (c) Magnified 1 μm × 1 μm image of $\varepsilon = 6.0$. The extension direction (ED) is indicated by an arrow.

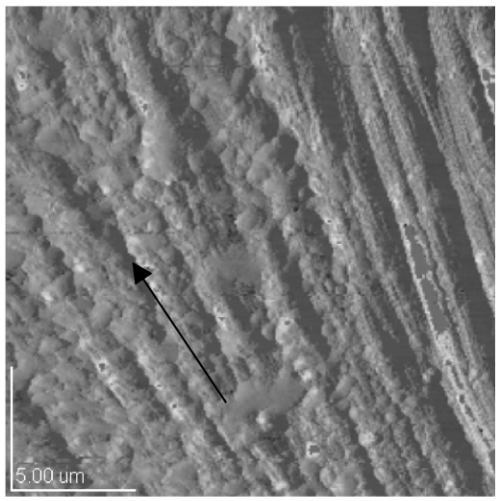

(a)

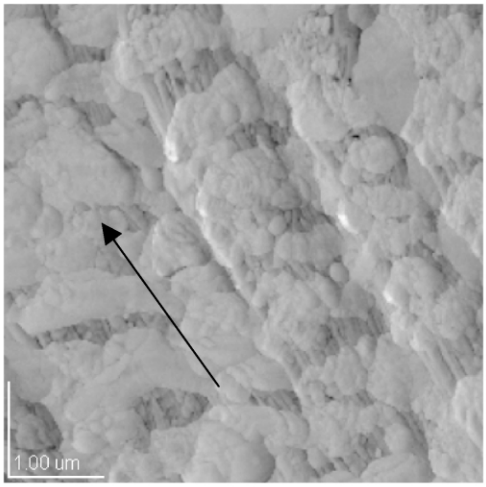

(b)

Fig. 7. Same as 6(b) when film is fully relaxed. (a) 20 μm × 20 μm image. (b) Magnified section of (a).

relaxed morphology resembles that of row-nucleated structures (shish-kebab) that are formed from oriented melts [23]. Alternating with a background-fibrillar morphology oriented in the direction of elongation, in each fiber there are blocks or rings of material that protrudes from the surface. These blocks, which are shown in detail in a magnified image in Fig. 7(b), most probably appeared as a consequence of retraction. This morphology is not observed in deformed and relaxed HDPEs and reveals the importance of the larger non-crystalline fraction in the deformation and relaxation process in LLDPE. We were unable to resolve the lamellar substructure in each of the LLDPE fibers by AFM.

The evolution of texture and lamellar morphology during deformation of the LLDPE contrasts with the texture of highly crystalline linear polyethylenes under uniaxial tension. The pole figures of the un-deformed HDPE and pole figures and orientation distribution plots of HDPE

stretched to a strain of 7.2 are given in Fig. 8, now with a grey texture scale comparable to that shown in Fig. 3 for LLDPE. Note that the use of orientation distribution plots allowed us to identify an extra texture component, (010)[001] that was not reported in our previous work [13]. The intensity of this component increased from 13.8 to 18 during deformation. The other five components of texture, shown in Fig. 8, were already discussed [13]. The (100)[001] component is the strongest in the deformed HDPE with intensity of 32.8. With increasing deformation, the texture evolved at a slow rate and the intensity of (103)[301] and (001)[010] decreased while the intensity of (014)[641] and (920)[010] increased. These components were labeled III, I, II, IV and V respectively in Ref. [13]. A combination of chain and transverse slip on the [010] direction were discussed to be the major driving force of the lamellar deformation. Active slips at 35–45° from the extension direction are related with the chain tilt in the lamellae [21]. From the evolution of the (001) pole in Fig. 8, it is obvious that a non-negligible fraction of the initial texture of HDPE remained up to the highest draw ratios.

The evolution of the lamellar morphology for HDPE during deformation is shown in Fig. 9 for the un-deformed (9a) and deformed specimens up to strains of 0.08 (9b), 1.0 (9c) and 4.0 (9d). The undeformed HDPE and deformed up to the yield point present identical lamellar arrangements as seen in Fig. 9(a),(b). Poorly organized spherulites made of short, curved lamellae prevail during the elastic reversible deformation as was also found in the lower crystallinity copolymer. Moreover, crystallization from a confined melt between the metal plates lent some orientation of crystallographic planes within the lamellar morphology of the original HDPE specimen. This was apparent from the texture observed in the pole figures of the un-drawn specimen (Fig. 8(a)). The copolymer with only 45% crystallinity did not develop any significant texture during crystallization from the confined melt suggesting that a reduced content of crystalline material favors a more

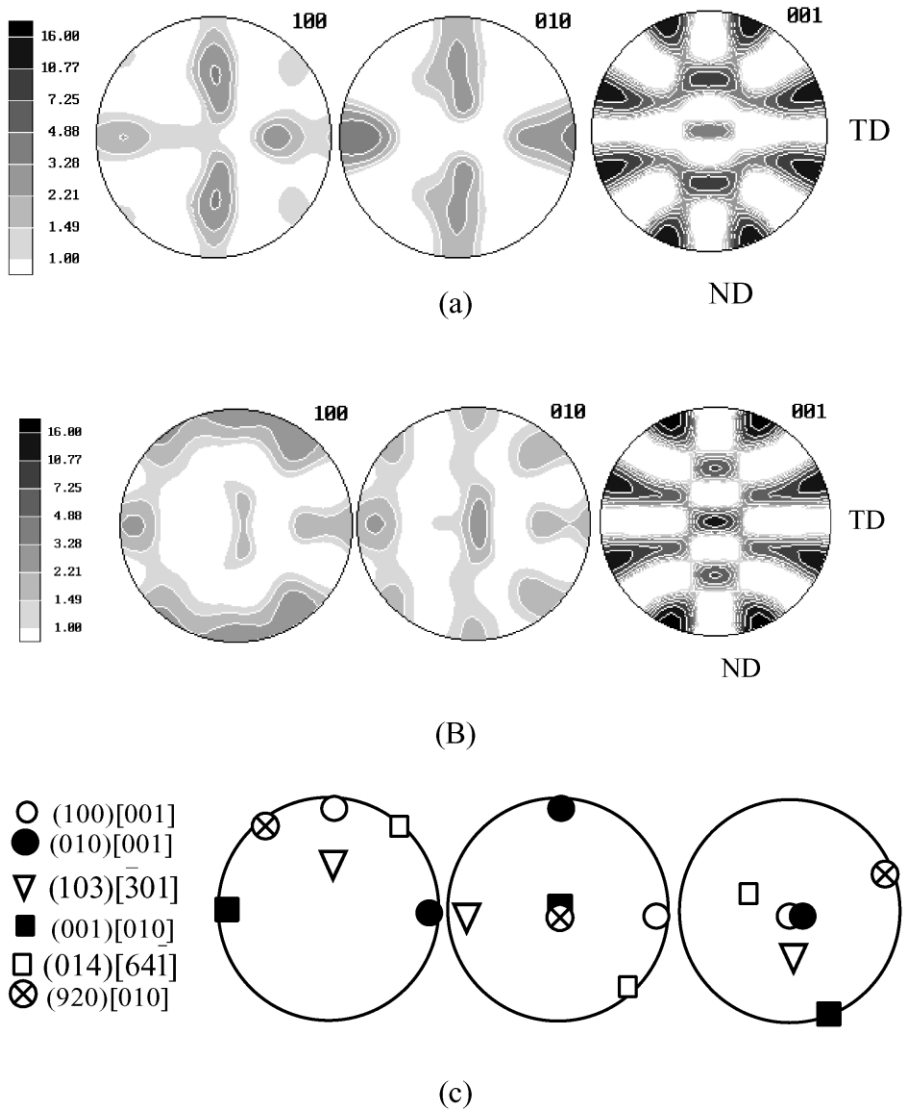

Fig. 8. Pole figures of the (100), (010), (001) planes of orthorhombic crystals of HDPE at strains of (a) 0, (b) 7.2, (c) orientation distribution plots of (b).

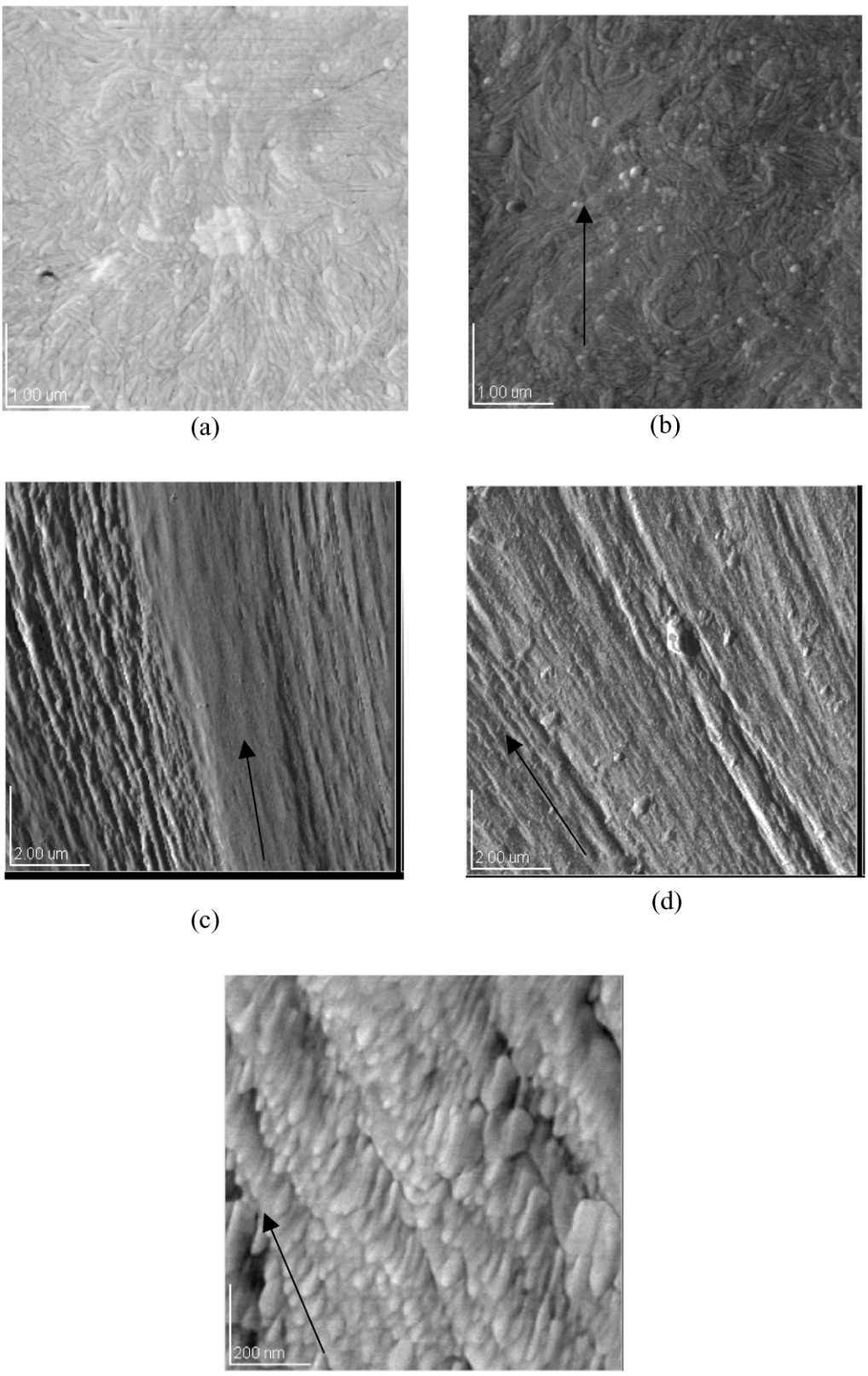

Fig. 9. AFM images of un-deformed and deformed HDPE at different strains. (a) $\epsilon = 0$, (b) $\epsilon = 0.08$, (c) $\epsilon = 1$, (d) $\epsilon = 4$, (e) magnified 1 μm × 1 μm image of (d). The extension direction is indicated by an arrow.

random orientation of the crystallites. A fibrillar structure is formed soon after yield, as seen in the image of Fig. 9(c) for $\varepsilon = 1.0$, and develops into well oriented fibers in the direction of elongation at higher levels of deformation (Fig. 9(d)). The fibers have diameters of 0.1–0.5 μ and are similar to those observed in high molecular weight polyethylene stretched to a draw ratio of 13.0 [24]. Interestingly, the sub-structure of the individual fibers was also resolved as shown in Fig. 9(e). Stacked lamellae are clearly the individual entities that form the fibers. Their long axis and *c*-axis of the lamellae are respectively perpendicular and parallel to the extension direction and their thicknesses are comparable to the thickness of the lamellae in the initial un-deformed specimen (~200 Å). The molecules in the lamellae are oriented in the extension direction supporting the notion that the majority of the crystalline deformation may have taken place by (100)[001] chain slip. The regularity of lamellar stacking in the fibers and the constancy of thicknesses with increasing strain lends support to the deformation mechanism by which, after yield, the irreversible transformation from lamellar to fibrillar structure occurs in a large extent via lamellae fragmentation and coarse chain slip. A few misaligned and flat-on lamellae are also observed in Fig. 9(e) and may be responsible for the additional weak components of texture.

3.2. Texture evolution during relaxation

Texture was measured at various time intervals, up to about two weeks after taking the polyethylenes out from the mechanical testing machine, while keeping the specimen at a constant imposed total strain level. Neither HDPE nor LLDPE showed any significant change in texture under this relaxation mode. To understand the differences in the relaxation process for these two types of polymer materials in this study, load relaxation experiments at constant strain were performed and stress history was monitored after the polyethylenes were stretched to a strain of 1.0 in/in. The results of the stress relaxation experiments are presented in Fig. 10(a),(b). In Fig. 10(a), the relative stress is plotted as a function of time for both HDPE (solid line) and ethylene l-octene copolymer (dashed line). The stresses are also plotted as a function of inelastic strain rates in Fig. 10(b) on a log–log scale. It is clear from Fig. 10(b) that stress in the copolymer relaxes at a much faster rate; the slope is larger in co-polymer than in HDPE. This difference in the relaxation behavior resulted in a stress drop to about 47% of the initial stress in 1000 s in LLDPE, while the corresponding stress drop in HDPE was only about 75%. These results reveal that during the WAXD data acquisition for the texture analysis, a substantial amount of the original stress in the copolymer was relaxed. Because changes in the microstructure and the resulting texture are partially governed by the stress within the intervening phases, it is not surprising that we found no significant differences in the pole figures of the copolymer at different strain levels after yield, as indicated in Fig. 3(b)–(d). In contrast, the stress in HDPE during the data acquisition process (at constant strain) is not very different from that during the deformation process.

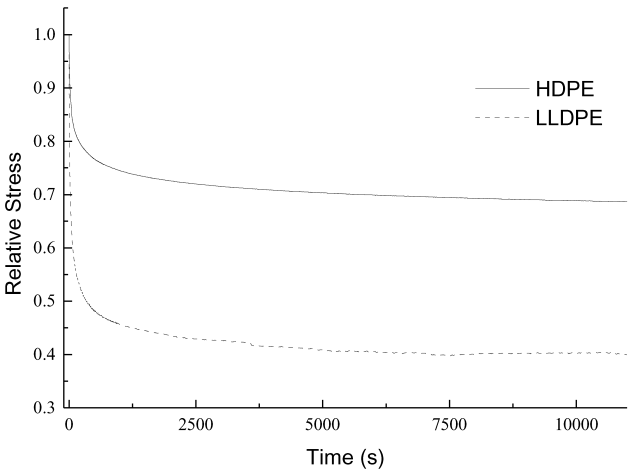

(a)

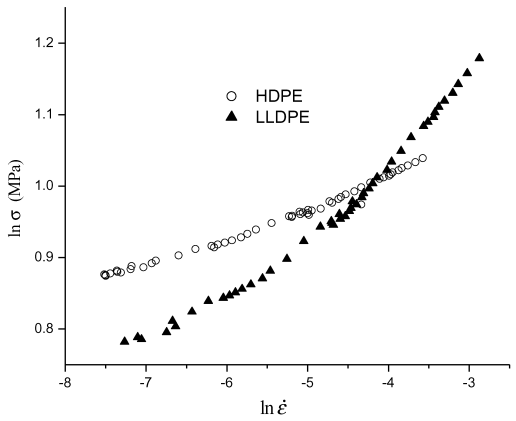

(b)

Fig. 10. (a) Plot of the relative stress versus time for HDPE and LLDPE at a constant strain of 1.0. (b) Plot of the log (stress) vs. log (inelastic strain rates) for HDPE and LLDPE at a constant strain of 1.0.

The texture of the copolymer subject to strains from 1.0 to 6.0 in./in. was basically indistinguishable between the loaded and relaxed samples. The pole figures of the samples unloaded and allowed to relax for three days were identical to those of Fig. 3. The intensity of (100)[001] orientation after relaxation was 8.4 times random compared to the 8.2 measured in the loaded (and then constrained for X-ray measurement) sample.

When a deformed linear polyethylene tensile sample was left to relax for three days its strain was reduced to 5.0 in./in. from 7.2 in./in. This had a major impact on the resulting texture. As shown in Fig. 11, the texture of the relaxed HDPE is quite different from the texture of the sample under load (Fig. 8(b)). The strong *c*-axis fiber component prevails

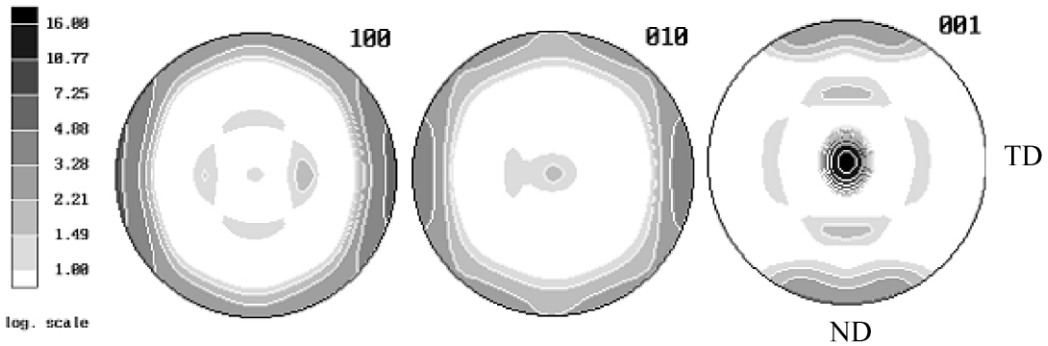

Fig. 11. Pole figures of the (100), (010), (001) planes of orthorhombic crystals of HDPE ($\varepsilon = 7.2$) after relaxation.

while the intensity of most other texture components is either eliminated or significantly diminished. The ODF of the relaxed HDPE corresponds quite accurately to the morphology of stacked lamella as individual entities of the fibers observed in the AFM image of Fig. 9(e). It is quite interesting that this is the reported texture for highly deformed polyethylenes in previous reports [5,25] suggesting that in these works the WAXD data may correspond to deformed and fully relaxed samples. Thus, not only were there major differences in the texture of the un-deformed HDPE and LLDPE, the changes in texture under relaxation are also quite different in both polyethylenes. Since stress relaxation under constant strain results in a small change in stress in HDPE, the measurements provide the texture of the sample during loading. After stress and strain were fully relaxed, significant changes in the texture were observed. The decrease of stress at a constant strain in ethylene copolymers is much larger and the texture levels off quickly at any point during the plastic deformation. Thus, only instantaneous acquisition of data to construct the pole figures would unquestionably resolve if the loaded LLDPE has a different texture than those shown in Fig. 3, and only in those conditions the mechanism of deformation of LLDPE may be properly constructed.

The observed behavior makes evident that the rate of texture evolution in the polyethylenes follows the rate of stress relaxation, which in turn follows the degree of crystallinity acquired by each type of polyethylene. The rate is relatively slow for HDPE and very fast in LLDPE of much lower crystallinity. In HDPE with high level of crystallinity, most of the stress remained in the constrained sample. Relaxation of the residual stress allowed further changes in the crystalline orientation and components with low texture are diminished or have disappeared. This is clearly reflected in the bar diagram of Fig. 12 where the evolution of the intensity of texture of the most prevalent components is illustrated for un-deformed, deformed and relaxed samples of LLDPE (Fig. 12(a)) and HDPE (Fig. 12(b)). Changes in the intensity of the components of the texture in deformed and relaxed LLDPE are insignificant. In HDPE the two main *c*-axis components (aligned with [001]) remain strong after stress and strain relaxation, while the intensity of the rest of the components decreased to very low values. Thus, the texture over the *c*-axis components intensified after unloading. One possible explanation is that after relaxation weakly oriented crystallites lose texture ending with a close to a random orientation distribution of crystallographic planes. It will be of interest to image the lamellar structure of HDPE specimens at large constant (and uniform) strains, but our attempts to do so were unsuccessful. The AFM images shown in Figs. 6 and 9 were collected on partially or totally relaxed samples and in both polyethylenes a fibrillar structure was clearly observed at different plastic strains. The strong *c*-axis fiber component observed after high levels of deformation is consistent with the texture measured by WAXD.

The mechanism of deformation appears to follow the slip and lamellar fragmentation steps as suggested in other studies [8,10]. This is quite evident for HDPE. Stacks of initially low textured lamellae retain their spherulitic integrity up to yielding. Beyond the yield region lamellar fragmentation occurs via longitudinal or other intralamellar or interlamellar slips. Blocks of fragmented lamellae reorient in the extension direction as a highly oriented fibrous structure. High crystallinity levels in HDPE may contribute to a prevailing intramolecular slip during deformation in agreement with the observed invariance of the long period during drawing. [4,10]. In LLDPE interlamellar slips may prevail because of the reduced crystallinity level, however, the true mechanism of transformation from the banded spherulitic structure to the fiber arrangement is unknown due to fast stress relaxation. The observed decrease of the long period during deformation [4] and the fast evolution of texture observed in the present study can be attributed to either melting of the original structure and re-crystallization during plastic deformation [26,27] or to profuse lamellar rotation and inter-lamellar slips. The experimental data do not allow distinction between the two mechanisms.

4. Conclusions

The evolution of texture in uniaxial tensile deformation of rapidly crystallized LLDPE (ethylene 1-octene) and HDPE was documented by the recalculated pole figures

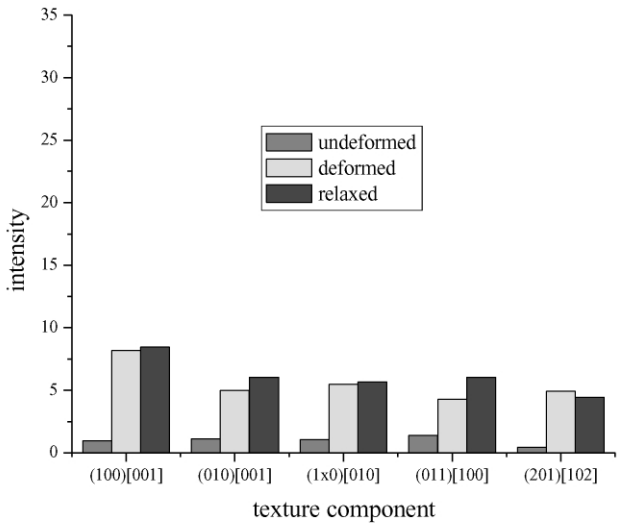

(a)

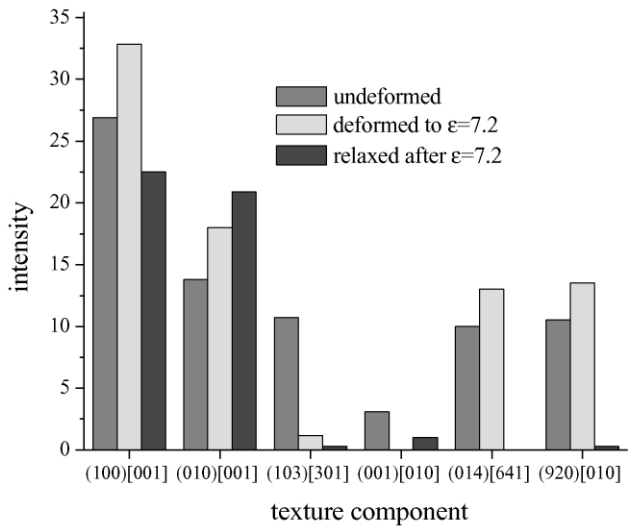

(b)

Fig. 12. Variation in normalized intensities of texture components (listed in Figs. 3 and 8) for un-deformed, deformed to a strain of 7.2 for HDPE and 1.0 for LLDPE and relaxed polyethylenes. (a) LLDPE (b) HDPE.

from the orientation distribution function (ODF) coefficients. The preferred deformation texture components in the linear polyethylene are (100)[001] and (010)[001]. AFM results showed that fibers form immediately after yield and the fibrilar structure aligns with the extension direction. Stacked segmented lamellae are the constituents of the individual fibers.

The initial texture of rapidly crystallized LLDPE is nearly random. In contrast with the behavior of HDPE, deformation of LLDPE past yield left no remnants of this initial texture and new texture components developed and stayed at about the same intensity in the whole plastic deformation region. The two main components were (100)[001] and (010)[001] with the *c*-axis aligned with the extension axis. A fibrillar morphology was also observed to form past yield and fully developed at the highest draw ratios, however the sub-structure of the individual fibers at the lamellar level was not resolved. Stress relaxation experiments at a constant strain documented that the stress of deformed LLDPE relaxes faster than that of HDPE. The difference in stress relation rates in turn explains the observed differences in measured textures between both types of polyethylenes.

Acknowledgements

The authors wish to acknowledge support by the National Science Foundation NSF grants#DMR-0094485 and DMR-9982872 and NASA Contract#NAGW-2930. The Center for Materials Research and Technology (MARTECH) of Florida State University is also acknowledged for additional funding for this research. Dr I.L. Hosier is acknowledged for assistance collecting some of the AFM images and helping with the etching procedure.

References

[1] Bartczak Z, Galeski A, Argon AS, Cohen RE. Polymer 1996;37:2113.
[2] Bartczak Z, Cohen RE, Argon AS. Macromolecules 1992;25:4692.
[3] Butler MF, Donald AM, Ryan AJ. Polymer 1997;38:5521.
[4] Butler MF, Donald AM, Ryan AJ. Polymer 1998;39:39.
[5] Pazur RJ, Ajji A, Prud'homme RE. Polymer 1993;34(19):4005.
[6] Bulter MF, Donald AM. J Appl Polym Sci 1998;67:321.
[7] Vickers ME, Fischer H. Polymer 1995;36(13):2667.
[8] Hiss R, Hobeika S, Lynn C, Strobl G. Macromolecules 1999;32:4390.
[9] Butler MF, Donald AM, Bras W, Mant GR, Derbyshire GE, Ryan AJ. Macromolecules 1995;28:6383.
[10] Peterlin A. J Mater Sci 1971;6:490.
[11] Lin L, Argon AS. J Mater Sci 1994;29:294.
[12] Bowden PB, Young RJ. J Mater Sci 1974;9:2034.
[13] Li D, Garmestani H, Kalidindi SR, Alamo RG. Polymer 2001;42:4903.
[14] Amornsakchai T, Olley RH, Bassett DC, Al-Hussein MOM, Unwin AP, Ward IM. Polymer 2000;41:8291.
[15] Bunn CW. Trans Faraday Soc 1989;35:483.
[16] Kallend JS, Kocks UF, Rollett AD, Wenk H-R. Mater Sci Engng 1991;A-132:1.
[17] Olley RH, Hodge AM, Bassett DC. J Polym Sci, Polym Phys Ed 1979; 17:627.
[18] Kennedy MA, Peacock AJ, Mandelkern L. Macromolecules 1994;27: 5297.
[19] Kennedy MA, Peacock AJ, Failla MD, Lucas JC, Mandelkern L. Macromolecules 1995;28:1407.
[20] Lu X, Qian R, Brown N. Polymer 1995;36:4239.
[21] Lu J, Sue H-J. Macromolecules 2001;34:2015.
[22] Butler JH, Wapp SM, Chambon EH. Adv X-Ray Anal 1999;43.
[23] Keller A. Proc R Soc Faraday Disc 1979;68:145.
[24] Li J, Lee Y-W. J Mater Sci 1993;28:6496.
[25] Garmestani H, Vaghar M, Hart EW. Int J Plast 2001;17:1367.
[26] Krause SJ, Hosford WF. J Polym Sci, Polym Phys Ed 1989;B27:1853.
[27] Flory PJ, Yoon DY. Nature 1978;272:226.
[28] Bartczak Z, Argon AS, Cohen RE. Macromolecules 1992;25:5036.